ISSN 0003-701X, Applied Solar Energy, 2022, Vol. 58, No. 4, pp. 461–465. © Allerton Press, Inc., 2022.
Russian Text © The Author(s), 2022, published in Geliotekhnika, 2022, No. 4, pp. 607–613.

SOLAR MATERIALS SCIENCE

Structural Properties of Sb_xSe_y Thin Films Obtained by CMBD for Solar Cells

T. M. Razykov[a], K. M. Kuchkarov[a, *], M. S. Tivanov[b], B. A. Ergashev[a], R. Khurramov[a], D. Z. Isakov[a], A. Olimov[a], D. S. Baiko[b], N. I. Polyak[b], O. V. Korolik[b], and S. D. Sharipov[b]

[a] *Physical–Technical Institute SPA Physics–Sun, Academy of Sciences of the Republic or Uzbekistan, Tashkent, 100084 Uzbekistan*

[b] *Belarusian State University, Minsk, 220030 Belarus*

**e-mail: k.kuchkarov@mail.ru*

Received September 15, 2022; revised October 7, 2022; accepted November 11, 2022

Abstract—Sb_xSe_y films were obtained by chemical molecular beam deposition (CMBD) on soda-lime glass substrates. Sb and Se were used as sources, their evaporation temperature was 950–1000°C (Sb) and 500°C (Se), the substrate temperature was maintained at about 500°C. Using scanning electron microscopy, X-ray diffraction analysis, and Raman scattering, the effect of the Sb/Se composition ratio on the structure of the synthesized films was studied. It was revealed that the films have a crystalline (orthorhombic) structure with compactly located crystallites having the form of rods with an average size: $l = 4–8$ μm (length) and $d = 2–3$ μm (diameter).

Keywords: Sb_2Se_3, Sb/Se, chemical molecular beam deposition, thin films, X-ray diffraction, Raman spectroscopy

DOI: 10.3103/S0003701X22040132

INTRODUCTION

Recently, the leading materials in the global photovoltaic market are Si, $Cu(In,Ga)Se_2$, and CdTe with an efficiency of 26.7, 23.35, and 21.0%, respectively [1].

Despite the widespread use of these materials, there are significant limitations to their use in the global production of photovoltaic modules. For example, the main disadvantage of Si-based solar cells is that silicon does not have an optimal band gap (1.1 eV) and has a low absorption coefficient ($\sim 10^2$ cm^{-1}), which increases the cost of the material, since it is required to use a material with a thickness of 100–200 microns [2]. At the same time, for thin-film solar cells based on $Cu(In,Ga,)Se_2$ and CdTe, their further large-scale application is complicated due to the limited amount of In and Ga in the Earth's crust, as well as the toxicity of cadmium (Cd), which is part of the solar cell structure [3].

Currently, world researchers are paying special attention to the use of chalcogenide binary compounds Sb_2Se_3, Sb_2S_3, and solid solutions $Sb_2(S_x,Se_{1-x})_3$ based on them (chemical formula Sb_2X_3) as an absorbing layer for solar cells [4]. This is due to the fact that the physical properties (*p*-type conductivity, band gap $E_g = 1.1–1.8$ eV, high absorption coefficient $\alpha > 10^5$ cm^{-1} in the visible region of solar radiation, low melting point (Sb_2Se_3, 823 K, Sb_2S_3, 885 K) and high partial pressure) of these materials are very close to the properties of $Cu(In,Ga)(Se,S)_2$ [4]. In addition, the elements included in these materials have a relatively low cost (common in nature), stability under external influences, and non-toxicity [5]. This will make it possible to produce environmentally friendly and efficient solar modules, and opens ways for their wide production on an industrial scale.

All these properties make Sb_2X_3 films competitive replacements for conventional absorbers (CdTe/CIGSe/CZTSe) in thin film solar cells. However, despite the above properties, films based on Sb_2X_3 are insufficiently studied. Recent research shows low efficiency of Sb_2X_3 based thin film solar cells compared to CdTe and CIGSe materials. Therefore, it is necessary to continue studying the structural properties of films based on Sb_2X_3, which will improve their efficiency in the future.

Sb_2Se_3 solar cell efficiency strongly depends on the physical properties of the base layer. To obtain the base layer in solar cells, chemical and physical methods are used: electrodeposition [6], successive ion-layer adsorption and reaction [7], chemical bath deposition [8], centrifugation [9], chemical vapor deposition using an aerosol [10], and physical methods (thermal evaporation [11], vacuum evaporation [12], fast thermal evaporation [13], vapor transport deposition [14],

Table 1. The chemical composition of the Sb_xSe_y films

T_{Se}, °C (temperature of selenium)	T_{Sb}, °C (antimony temperature)	Sb (atomic percent %)	Se (atomic percent %)	Sb/Se (atomic ratio)
500	950	46	54	0.85
	960	40	60	0.66
	990	42	58	0.72
	1000	43	57	0.75

magnetron sputtering [15], and sublimation in a closed volume [16]).

Previously, we studied the structural and morphological properties of Sb_2Se_3 films obtained by the chemical molecular beam deposition (CMBD) from powders of binary compound Sb_2Se_3 at different substrate temperatures. The results showed that all the films were enriched in antimony and had an orthorhombic structure with predominant [120] and [221] orientations; the crystallite sizes of the films were 200–300 nm [17].

In this study, we analyze the structural properties of Sb_xSe_y obtained by CMBD from separate sources of Sb and Se elements at a substrate temperature of 500°C.

METHODS AND MATERIALS

Preparation of Sb_xSe_y films by CMBD is described in detail in [18]. Sb and Se materials of semiconductor purity (99.999%), which were evaporated in a hydrogen flow at atmospheric pressure, were used as the starting material. The evaporation temperature range of Sb and Se materials for film growth was within 950–1000°C for Sb, and 500°C for Se, the substrate temperature was maintained at 500°C. The hydrogen carrier gas flow was about 20 cm^3/min. The duration of the deposition process was 30 min. Soda-lime glass was used as substrates. The dimensions of the samples were 2.0 × 2.0 cm^2. To obtain Sb_2Se_3 films with a stoichiometric composition, the partial pressure of Sb in the vapor phase changed during the growth process.

Elemental (chemical) composition of the synthesized Sb_xSe_y films was determined by energy-dispersive X-ray spectroscopy (EDX) using an Aztec Energy Advanced X-Max 80 energy-dispersive nitrogen-free spectrometer. The surface morphology features were studied using an LEO-1455 VP scanning electron microscope. X-ray diffraction patterns were taken on a Rigaku Ultima IV high-resolution diffractometer in the range of angles $2\theta = 10°–60°$ with a wavelength of CuK_α-radiation of 0.15418 nm. Phase identification was carried out by comparing the experimentally found interplanar distances with tabular values from the database of the Joint Committee for Powder Diffraction Standards (JCPDS). The Raman spectra were measured at room temperature using a Nanofinder HE (LOTIS TII) confocal spectrometer. For excitation, a solid-state laser with a wavelength of 532 nm was used. Laser radiation with a power of 60 μW was focused on the surface of the samples to a region about 0.7 μm in diameter.

RESULTS AND DISCUSSION

The chemical composition of the samples, determined by EDX, is presented in Table 1. It can be seen that the synthesized films consist of antimony and selenium, while the Sb content varies in the range of 40–46 at %, the rest is Se, i.e., the ratio of these components is close to 2 : 3 and, in accordance with the state diagram of the Sb–Se system, the presence of the Sb_2Se_3 phase can be expected in the films [19].

Figure 1 shows X-ray diffraction patterns of thin films with different Sb/Se ratios. All thin films have noticeable peaks that are in good agreement with the standard JCPDS card (No. 15–0861) of the orthorhombic Sb_2Se_3 phase. As can be seen from the figure, strong peaks (221) and (211) and weak peaks (020), (120), and (310) are observed in the diffraction patterns the intensity of which changes noticeably with the Sb temperature. According to [20], Sb_2Se_3 mainly consists of ribbons $(Sb_4Se_6)n$ in the form of one-dimensional chain structures. Ribbons $(Sb_4Se_6)n$ are superimposed on each other in the [001] direction due to strong Sb–Se covalent bonds. However, in the [100] and [010] directions, the ribbons are bound by van der Waals forces [21–23]. Media migration across $(Sb_4Se_6)n$ tapes occurs much faster than between ribbons [24, 25]. Therefore, to ensure efficient carrier transfer, it is especially important to control the growth orientation of Sb_2Se_3 thin films. It is obvious that the series resistance in grains with [120] orientation is much higher than in grains with [211] and [221] orientations. Therefore, to promote carrier transport and improve solar cell performance, these $(Sb_4Se_6)n$ ribbons should grow perpendicular to the substrate, for example, in the [211] or [221] direction.

For more information about the structural properties of Sb_xSe_y films obtained by CMBD at a substrate temperature of 500°C, with different Sb/Se ratio (0.85; 0.73; 0.66), Raman spectra were measured (Fig. 2). As can be seen from Fig. 2, the Raman spectra of all films exhibit peaks characteristic of Sb_2Se_3: 62, 78–80, 100,

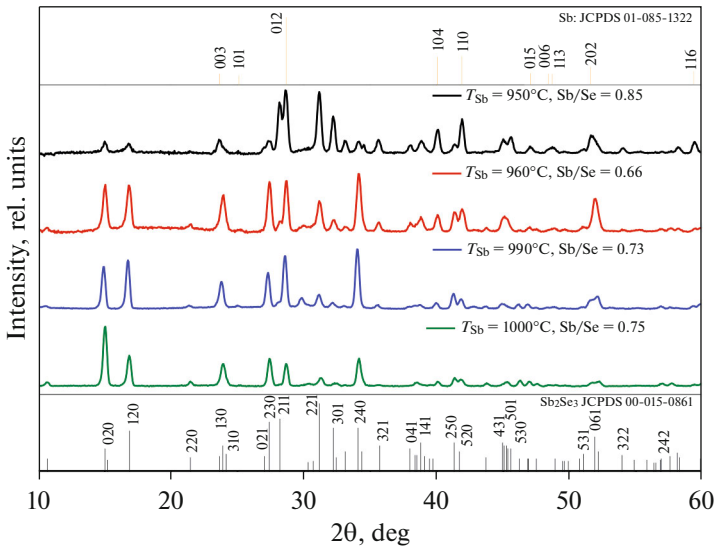

Fig. 1. X-ray diffraction patterns of Sb_2Se_3 films of different composition, obtained at different temperatures of the antimony source.

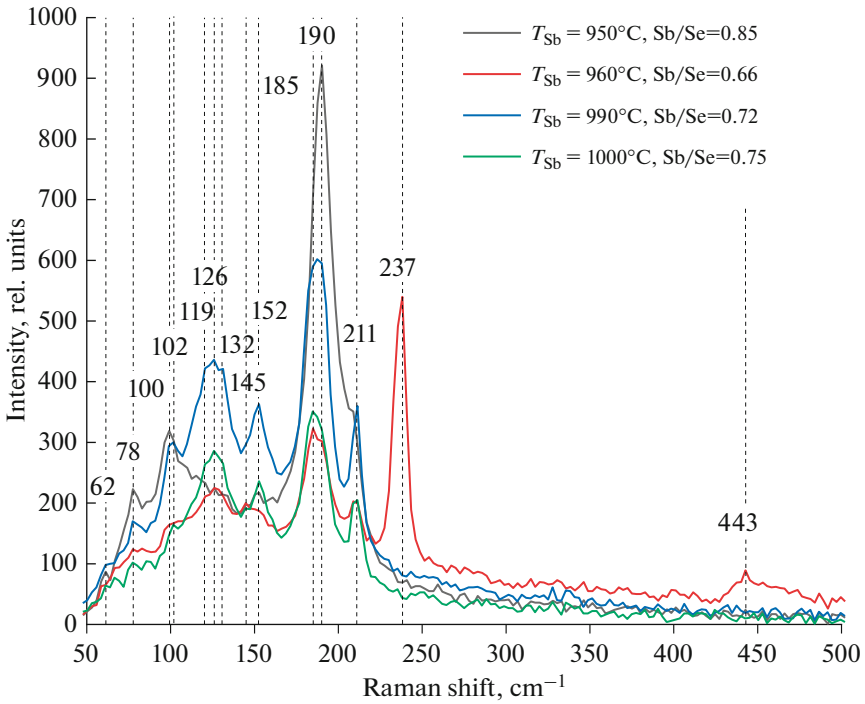

Fig. 2. Raman spectra of Sb_2Se_3 films of different composition synthesized at different temperatures of the Sb source.

102, 119, 126, 132, 151–153, 184–186, 190–193, and 211 cm^{-1} [26]. However, for a film with a Sb/Se ratio of 0.66, peaks at 145, 237, and 443 cm^{-1} are also observed in the Raman spectrum, characteristic of trigonal Se. Thus, the Raman results allow us to speak about the formation of the main phase in the Sb_2Se_3 films and secondary phase Se.

Surface morphology and cross section studies (with the cross section in each figure shown in the upper right corner) of Sb_2Se_3 films of different composition, carried out using scanning electron microscopy, obtained at different temperature ranges of Sb, at which the temperature of Se remains relatively unchanged, are shown in Fig. 3. It was found that their

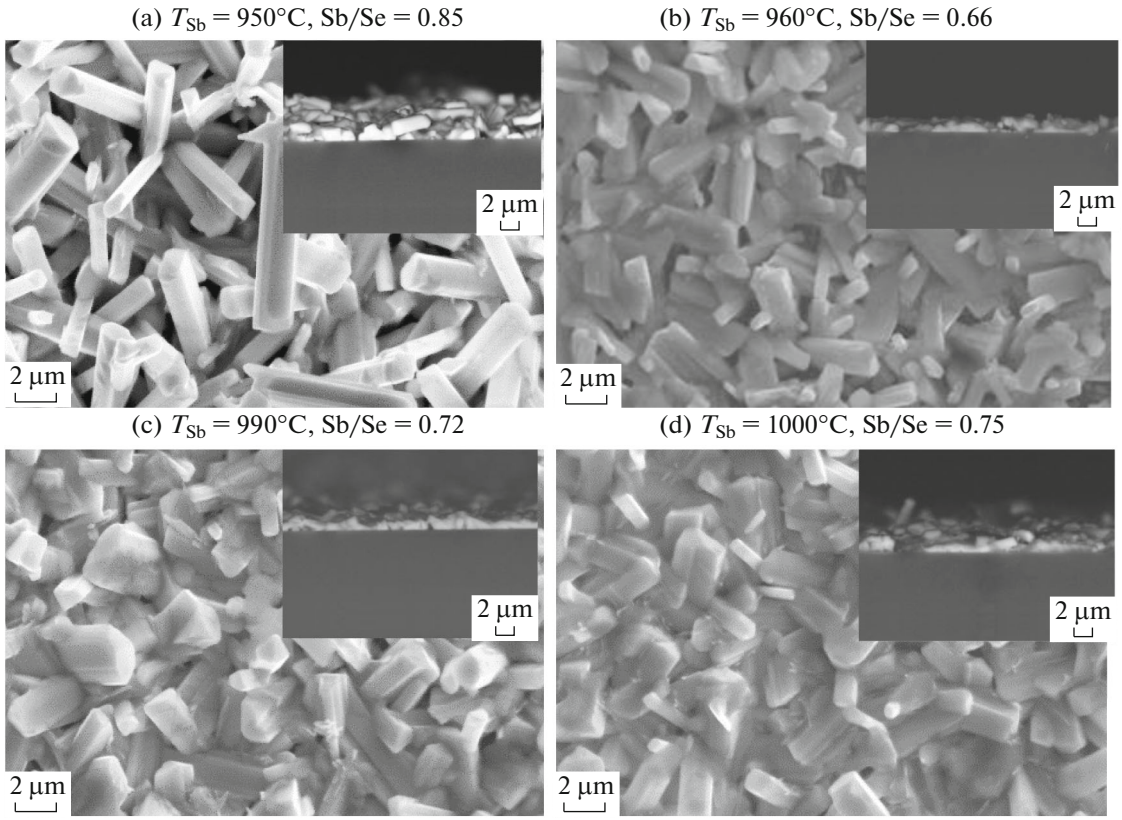

Fig. 3. Surface morphology of Sb_2Se_3 films of different composition at different temperatures of the antimony source, obtained on a scanning electron microscope.

structure consists mainly of randomly located rods, which, depending on T_{Sb} have a different inclination with respect to the substrate, differ in size, density of their arrangement, and the presence or absence of microvoids and microcracks.

As can be seen from Fig. 3, all Sb_2Se_3 film samples of different composition have a dense columnar structure.

For films with T_{Sb} = 950°C (Fig. 3a), a columnar structure with a diameter d = 1–2 μm and length l = 4–8 μm was obtained. The tilt of the rods is from 0° to 45° relative to the substrate surface, the film thickness is about 2 μm (Fig. 3a). Films with T_{Sb} = 960°C (Fig. 3b) have a finer columnar structure (d = 0.5–2 μm, l = 2–4 μm). Tilt of rods up to 30° and film thickness about 1 μm (Fig. 3b, cross-sectional SEM image).

Samples with the highest T_{Sb} values (Figs. 3c and 3d) practically do not differ from each other, they have the smallest length of the rods (l = 2–3 μm) among all samples and the same diameter spread as samples with lower source temperatures of Sb, however, the proportion of small rods with d = 0.5–1.0 μm is negligible. The angle of inclination relative to the substrate mainly lies in the range from 0° to 30°, the thickness of the films is in the range of 1.0–1.2 μm (Figs. 3c and 3d).

CONCLUSIONS

Sb_2Se_3 films with different Sb/Se ratios have been obtained by CMBD from separate sources of Sb and Se elements at a substrate temperature of 500°C.

The results of scanning electron microscopy and X-ray diffraction analysis showed that all films have an orthorhombic structure with predominant (211) and (221) orientations; the crystallite sizes of the films are l = 4–8 μm and d = 2–3 μm. The results of Raman spectroscopy confirmed the formation of the main phase in Sb_2Se_3 films, however, for a film with a ratio of Sb/Se of 0.66, the presence of a side phase, trigonal Se, was found.

FUNDING

This study was supported by the Fundamental Research Program of the Academy of Sciences of the Republic of Uzbekistan and the State Committee on Science and Technology of the Republic of Belarus (grant no. F21UZBG-022).

CONFLICT OF INTEREST

The authors declare that they have no conflicts of interest.

REFERENCES

1. Green, M.A., et al., Solar cell efficiency tables (Version 58), *Prog. Photovoltaics,* 2021, vol. 29, pp. 657–667.
2. Razykov, T.M., Ferekides, C.S., et al., Solar photovoltaic electricity: Current status and future prospects, *Sol. Energy,* 2011, vol. 85, pp. 1580–1608.
3. Dhere, N.G., Scale-up issues of CIGS thin film PV modules, *Sol. Energy Mater. Sol. Cells,* 2011, vol. 95, pp. 277–280.
4. Xiaomin, W., Rongfeng, T., and Chunyan, W., Development of antimony sulfide–selenide $Sb_2(S,Se)_3$-based solar cells, *J. Energy Chem.,* 2018, vol. 27, pp. 713–721.
5. Mavlonov, A., Razykov, T., Raziq, F., et al., A review of Sb_2Se_3 photovoltaic absorber materials and thin-film solar cells, *Sol. Energy,* 2020, vol. 201, pp. 227–246.
6. Kwon, Y.H., Kim, Y.B., Jeong, M. et al., Crystal growth direction-controlled antimony selenide thin film absorbers produced using an electrochemical approach and intermediate thermal treatment, *Sol. Energy Mater. Sol. Cells,* 2017, vol. 172, pp. 11–17.
7. Weihuang, W., Xiaomin, W., Guilin, Ch., et al., Deposition of metal chalcogenide thin films by successive ionic layer adsorption and reaction (SILAR) method, *Bull. Mater. Sci.,* 2004, vol. 27, no. 2, pp. 85–111.
8. Kulkarni, A., Arote, S., Pathan, H., et al., Sb_2Se_3 sensitized heterojunction solar cells, *Mater. Renewable Sustainable Energy,* 2015, vol. 4, no. 1, p. 15.
9. Zhou, Y., Leng, M., Xia, Z., et al., Solution-processed antimony selenide heterojunction solar cells, *Adv. Energy Mater.,* 2014, vol. 4, p. 1301846.
10. Khan, M.D., Aamir, M., Sohail, M., et al., Novel single source precursor for synthesis of Sb_2Se_3 nanorods and deposition of thin films by AACVD: Photo-electrochemical study for water reduction catalysis, *Sol. Energy,* 2018, vol. 169, p. 526.
11. Liu, X., Chen, J., Luo, M., et al., Thermal evaporation and characterization of Sb_2Se_3 thin film for substrate Sb_2Se_3/CdS solar cells, *ACS Appl. Mater. Interfaces,* 2014, vol. 6, p. 10687.
12. Mustafa, F.I., Gupta, S., Goyal, N., et al., Effect of temperature on the optical parameter of amorphous Sb-Se thin films, *J. Optoelectron. Adv. Mater.,* 2019, vol. 11, no. 12, pp. 2019–2023.
13. Wang, L., Li, D.B., Li, K., Chen, C., et al., Stable 6%-efficient Sb_2Se_3 solar cells with a ZnO buffer layer, *Nat. Energy,* 2017, vol. 2, no. 4, p. 17046.
14. Liu, X., Xiao, X., Yang, Y., et al., Enhanced Sb_2Se_3 solar cell performance through theory-guided defect control, *Prog. Photovoltaics: Res. Appl.,* 2017, vol. 25, no. 10, pp. 861–870.
15. Liang, G.X., Zhang, X.H., Ma, H.L., et al., Facile preparation and enhanced photoelectrical performance of Sb_2Se_3 nanorods by magnetron sputtering deposition, *Sol. Energy Mater. Sol. Cells,* 2017, vol. 160, pp. 257–262.
16. Hutter, O.S., Phillips, L.J., Yates, P.J., et al., CSS antimony selenide film morphology and high efficiency PV devices, *2018 IEEE 7th World Conference on Photovoltaic Energy Conversion (WCPEC) (A Joint Conference of 45th IEEE PVSC, 28th PVSEC & 34th EU PVSEC),* 2018, pp. 0027–0031.
17. Razykov, T.M., Shukurov, A.Kh., Kuchkarov, K.M., et al., Morphological and structural characteristics of Sb_2Se_3 thin films fabricated by chemical molecular beam deposition, *Appl. Sol. Energy,* 2019, vol. 55, pp. 376–379.
18. Razykov, T.M., Chemical molecular beam deposition of II-VI binary and ternary compound films in gas flow, *Appl. Surf. Sci.,* 1991, vols. 48/49, no. 1, pp. 89–92.
19. Hongwei, L., Jianjun, Ch., Zuojun, T., and Guojia, F., Review of recent progress in antimony chalcogenide-based solar cells: Materials and devices, *Sol. RRL,* 2019, vol. 3, no. 6, p. 1900026.
20. M. Wobst, Investigation of the miscibility gaps in the binary systems silver-tellurium, indium-tellurium, gallium-tellurium, thallium-tellurium and antimony-selenium, *Scr. Metall.,* 1971, vol. 5, no. 7, pp. 583–585.
21. Wang, D., Song, C., Fu, X., and Li, X., Growth of one-dimensional Sb_2S_3 and Sb_2Se_3 crystals with straw-tied-like architectures, *J. Cryst. Growth,* 2005, vol. 281, pp. 611–615.
22. Deringer, V.L., Stoffel, R.P., Wuttig, M., and Dronskowski, R., Vibrational properties and bonding nature of Sb_2Se_3 and their implications for chalcogenide materials, *Chem. Sci.,* 2015, vol. 6, pp. 5255–5262.
23. Zhou, Y., Li, Y., Luo, J., Li, D., Liu, X., Chen, C., Song, H., Ma, J., Xue, D.-J., Yang, B., and Tang, J., Buried homojunction in CdS/Sb_2Se_3 thin film photovoltaics generated by interfacial diffusion, *Appl. Phys. Lett.,* 2017, vol. 111, p. 013901.
24. Li, D.B., Yin, X., Grice, C.R., Guan, L., Song, Z., Wang, C., Chen, C., Li, K., Cimaroli, A.J., Awni, R.A., Zhao, D., Song, H., Tang, W., Yan, Y., and Tang, J., Stable and efficient CdS/Sb_2Se_3 solar cells prepared by scalable close space sublimation, *Nano Energy,* 2018, vol. 49, pp. 346–353.
25. Zhou, Y., Wang, L., Chen, S., Qin, S., Liu, X., Chen, J., Xue, D.J., Luo, M., Cao, Y., and Cheng, Y., Thin-film Sb_2Se_3 photovoltaics with oriented one-dimensional ribbons and benign grain boundaries, *Nat. Photonics,* 2015, vol. 9, pp. 409–415.
26. Pedro, V.F., Maxim, G., et al., Multiwavelength excitation Raman scattering study of Sb_2Se_3 compound: Fundamental vibrational properties and secondary phases detection, *2D Mater.,* 2019, vol. 6, p. 045054.